

# Engineering V-Type Nerve Agents Detoxifying Enzymes Using Computationally Focused Libraries

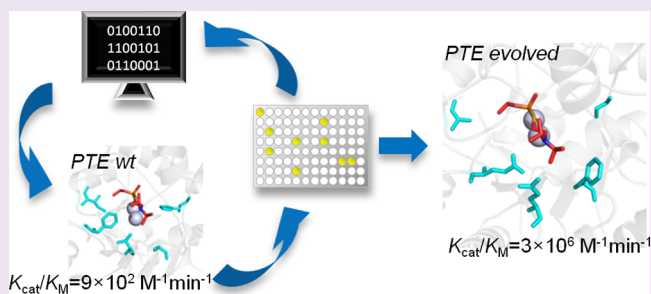
Izhack Cherny,<sup>†,§</sup> Per Jr. Greisen,<sup>‡,§</sup> Yacov Ashani,<sup>†</sup> Sagar D. Khare,<sup>‡</sup> Gustav Oberdorfer,<sup>‡</sup> Haim Leader,<sup>†</sup> David Baker,<sup>\*,‡</sup> and Dan S. Tawfik<sup>\*,†</sup>

<sup>†</sup>Department of Biological Chemistry, Weizmann Institute of Science, Rehovot 76100, Israel

<sup>‡</sup>Department of Biochemistry, University of Washington, Seattle, Washington 98195, United States

## Supporting Information

**ABSTRACT:** VX and its Russian (RVX) and Chinese (CVX) analogues rapidly inactivate acetylcholinesterase and are the most toxic stockpile nerve agents. These organophosphates have a thiol leaving group with a choline-like moiety and are hydrolyzed very slowly by natural enzymes. We used an integrated computational and experimental approach to increase *Brevundimonas diminuta* phosphotriesterase's (PTE) detoxification rate of V-agents by 5000-fold. Computational models were built of the complex between PTE and V-agents. On the basis of these models, the active site was redesigned to be complementary in shape to VX and RVX and to include favorable electrostatic interactions with their choline-like leaving group. Small libraries based on designed sequences were constructed. The libraries were screened by a direct assay for V-agent detoxification, as our initial studies showed that colorimetric surrogates fail to report the detoxification rates of the actual agents. The experimental results were fed back to improve the computational models. Overall, five rounds of iterating between experiment and model refinement led to variants that hydrolyze the toxic  $S_p$  isomers of all three V-agents with  $k_{cat}/K_M$  values of up to  $5 \times 10^6 \text{ M}^{-1} \text{ min}^{-1}$  and also efficiently detoxify G-agents. These new catalysts provide the basis for broad spectrum nerve agent detoxification.



Organophosphate pesticides and chemical warfare nerve agents (Figure 1) covalently inhibit acetylcholinesterase (AChE) and cause cholinergic overstimulation of synapses. Intoxication is currently treated by attempting to reverse AChE

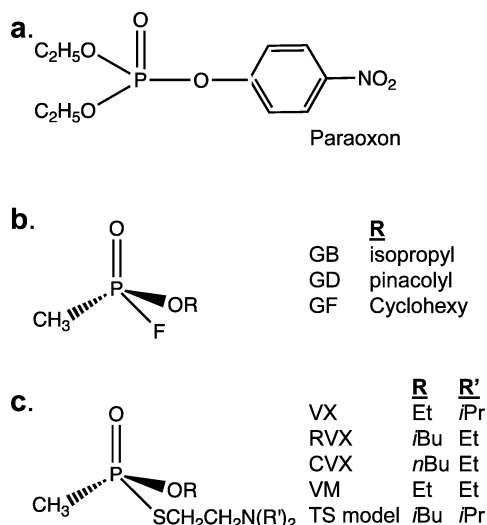


**Figure 1.** Organophosphates used in this study (for a complete scheme see Supplementary Figure 7). (a) Paraoxon. (b) G-type nerve agents, toxic  $S_p$  isomer. (c) V-type nerve agents, toxic  $S_p$  isomer.

inhibition with oximes.<sup>1</sup> A better option would be to intercept the organophosphates (OPs) prior to their interaction with AChE. Butyrylcholinesterase is an option but acts stoichiometrically, thereby demanding impractically high enzyme doses.<sup>2</sup> An optimal solution would be a multiple turnover hydrolase,<sup>3</sup> but such would have to display catalytic efficiency ( $k_{cat}/K_M$ ) that exceeds  $10^7 \text{ M}^{-1} \text{ min}^{-1}$ .<sup>4</sup> OPs are coincidental substrates for natural hydrolases and are therefore hydrolyzed at low rates. A notable exception is PTE, an enzyme found in soil bacteria.<sup>5</sup> Paraoxon (Figure 1a) appears to be the natural substrate of PTE and is hydrolyzed with  $k_{cat}/K_M$  of  $2.0 \times 10^9 \text{ M}^{-1} \text{ min}^{-1}$ , thus making PTE an ideal candidate for *in vivo* detoxification and environmental decontamination of paraoxon and related pesticides.

Nerve agents (NAs), however, differ significantly from paraoxon (Figure 1b,c). First, they are mostly methylphosphonates rather than dialkylphosphate esters. Second, they possess a chiral phosphorus with the  $S_p$  isomer being the toxic component. The detoxification rates (i.e., rates of hydrolysis of the toxic  $S_p$  isomers) of NAs by enzymes such as PTE are generally orders-of-magnitude lower than for paraoxon. To improve catalytic rates, enzyme engineering can be applied.

**Received:** July 3, 2013

**Accepted:** September 16, 2013

**Published:** September 16, 2013

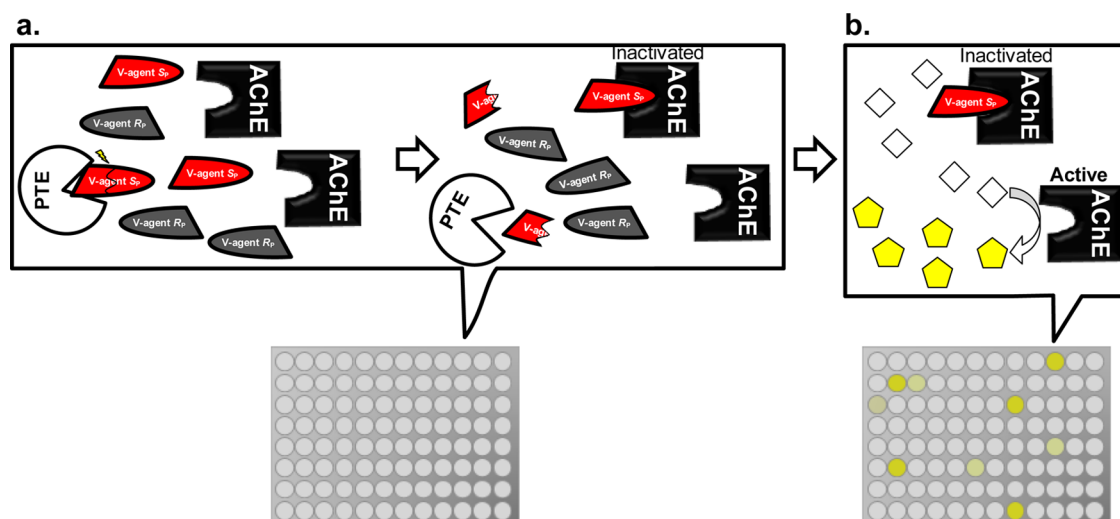


**Figure 2.** The AChE protection screen. *E. coli* clones, each expressing a different PTE variant, were grown and lysed in 96-well plates. (a) Acetylcholine esterase (AChE) is added to the lysates, followed by the nerve agent. (In the first generations, G1–G3, the *preincubation* mode was applied, i.e., lysates were first incubated with the V-agent for 30 min, and AChE was subsequently added.) The presence of a PTE variant that efficiently degrades the toxic  $S_p$  isomer is detected by virtue of prevention of AChE's irreversible inhibition. (b) The residual AChE activity is monitored by a chromogenic assay (measuring the release of free thiol group, using acetylthiocholine substrate and Ellman's reagent). Variants showing the highest AChE activity were purified, kinetically characterized, and used as the basis for the next generation.

Using directed evolution, we increased human serum paraoxonase (PON1) detoxification rates with GD and GF (the deadliest G-agents) by  $\leq 3400$ -fold, to  $k_{\text{cat}}/K_M$  values  $\geq 3 \times 10^7 \text{ M}^{-1} \text{ min}^{-1}$ , thus enabling prophylactic protection at low protein doses ( $\leq 1 \text{ mg enzyme/kg body weight}$ ).<sup>6</sup> PTE has been similarly engineered to detoxify GF.<sup>7</sup>

In contrast to paraoxon and G-agents, V-agents possess a thioleaving group (Figure 1c). The poorer hydrogen-bonding ability of sulfur relative to oxygen and the lower electrophilicity of the phosphorus make V-agents inferior substrates for hydrolases including PTE.<sup>8</sup> Indeed, as described below, PTE's hydrolysis rates of oxo-esters are  $>1000$ -fold faster relative to thio-esters with the same leaving group  $\text{p}K_a$  value (the thio-effect). Stereospecificity is another obstacle. While toxicity relates to the  $S_p$  isomer, the available measurements regard only racemic VX or RVX and report similar  $k_{\text{cat}}/K_M$  values for both agents ( $\sim 10^4 \text{ M}^{-1} \text{ min}^{-1}$ ).<sup>8</sup> However, we found that while PTE's hydrolysis rate of both isomers of VX is similar, the toxic  $S_p$  isomer of RVX is hydrolyzed  $\sim 30$ -fold more slowly than its  $R_p$  isomer. Overall, PTE's  $k_{\text{cat}}/K_M$  values need to be improved by  $>10^4$ -fold for effective *in vivo* detoxification of V-agents. PTE has been subjected to engineering, but the demonstrated improvements related mostly to surrogates, to racemic VX, or to VX alone rather than the entire range of V-agents.<sup>7–13</sup> Engineering has also failed to address the choline-like tertiary ammonium group, a unique feature of V-agents, and the challenge of detoxifying the entire range of V-agents beyond VX.

## RESULTS AND DISCUSSION

The aim of the study was to engineer PTE for broad-spectrum V-agent detoxification. To this end, we developed a direct screen for the detoxification of the entire range of known V-agents combined with a computational method to guide library design.

**Experimental Platform: AChE Rescue Screen.** Success in enzyme engineering depends on being able to screen large libraries or to correctly predict mutations that trigger the

desired activity. Detoxification of V-agents presents a major hurdle for high-throughput screens ( $>10^3$  variants). Chromogenic surrogates are a common option.<sup>11,12,14</sup> Surrogates, however, report only some molecular features of V-agents and may fail to reflect the actual detoxification rates. Additionally, to avoid selection of variants preferring the  $R_p$  isomers, the screen must be performed with pure  $S_p$  isomer. We have therefore opted for a detoxification assay using the V-agents at nonhazardous concentrations. The assay mimics the *in vivo* challenge, where the detoxifying variant must hydrolyze the  $S_p$  isomer at submicromolar concentrations before it binds and inhibits AChE. The latter occurs at a second-order rate of  $\sim 10^8 \text{ M}^{-1} \text{ min}^{-1}$ . Following previous developments in our lab,<sup>6</sup> we developed a screen based on measuring residual AChE activity after exposure to V-agents (Figure 2). While the assay uses racemic agents, only hydrolysis of the  $S_p$  component rescues AChE.

Several steps were taken to establish this screen. First, the *in situ* synthesis of V-agents from two nonhazardous components, the respective *O*-alkyl methylphosphonothiolate and 2-(*N,N*-dialkylamino)ethyl chloride, was developed. Mixing these precursors in aqueous solution gave the required V-agents in amounts that are  $\leq 1/30$  of the assumed percutaneous LD50. Second, conditions for performing the assay with crude bacterial lysates expressing the enzyme variants were established. A *preincubation* mode was necessary to detect detoxification by wild-type PTE (V-agents incubated with the lysate before addition of AChE). As more active enzyme variants were obtained, *coincubation* mode was applied: V-agents were added to a mixture of AChE and lysate, and AChE residual activity was subsequently measured. Upon overexpression of the wild-type-like variant PTE-S5 (described below), only low levels of protection against RVX could be detected ( $\sim 7\%$  residual AChE activity, upon preincubation of 3 nM RVX with 50  $\mu\text{L}$  of lysate of *E. coli* cells expressing PTE-S5). Clear protection against VX could be observed ( $\geq 70\%$ ) and weaker protection against CVX ( $\sim 20\%$ ). These protection levels are in agreement with PTE-S5's  $k_{\text{cat}}/K_M$  values with the  $S_p$  isomers of the three agents (described below).

Table 1. Library Compositions of the Five Rounds of Optimization

round	spiked library mutations	rationale	mutations found in most active variants
G1	G60AV, I106AGCL, W131HQYFA, F132HQYWA, H254QNR, H257WFYL, L271YIM, L303IMC, F306LIWF, S308GA, Y309WF, M317IL	Previous reports of engineered PTE variants <sup>a</sup>	I106A, W131H, F132A, H245NQR, L271Y
	G60H, S61G, I106AG, W131H, A171ST, H245NQ, H257W, L271Y, L303ITV, S308G, Y309S	Computationally identified active-site mutations	I106A, W131H, A171S, H245NQ, L271Y, L303TV
	K77A, A80V, S111R, I274S, A204G	Stabilizing, compensatory mutations	K77A, A80V, S111R, I274S, A204G
	R185K, G208D, S319R	Increased metal stability (reverting S5 to wild-type PTE)	R185K, G208D, S319R
G2	D233MQETNSC, H254X, H257MIRKLFY	Neighbor joining (combinations of 254 and its neighboring residues)	H254G
	C59AST, W131NDH, L136VAST, F132DE, T103AG, I271HQNK, F306RKT, S308HQNK	Test of an alternative model of VX/RVX complexes	F132DE
	M317WA		none
G3	W131X, F132I	Neighbor joining (exploring combinations of 131 and the neighboring 132).	none
	T147Y, Q295Y, M314H, D315V	Computationally predicted stabilizing mutations	T174Y
	I274N	A reported stabilizing mutation <sup>b</sup>	I274N
G4	C59YFAVLP, G60AP, S61DEGA, D105NQSAP, I106V, W131YFG, D133RKHSA, D233EKNQMILV, I255MFY, P256G, H257Y, S258QN	Revisiting mutated positions and neighboring positions	C59VF, S61G, I106V, D233M, H257Y, S258N
G5	T173NYQW, A203LIVFMWY	Computationally identified active-site mutations	T173NQ, A203FL
	H254ST Loop 7 single amino acid deletions (residue 256–259, 265–273)	Loop7 remodeling	H254S A266 del

<sup>a</sup>References 8, 10, 11, 16–18, and 20–22. <sup>b</sup>Reference 31.

Finally, we have designed an assay to address metal composition and affinity. PTE has a bimetallo catalytic site that accepts a range of transition metals.<sup>15</sup> The cobalt form is probably the most active one and is often used with NAs, including V-agents.<sup>7,8,16–18</sup> However, in view of the potential *in vivo* applications, we used zinc, the most abundant transition metal in serum ( $\geq 10 \mu\text{M}$ , 3000-fold higher than cobalt). Following growth of the enzyme expressing *E. coli* cells in zinc contacting medium, lysis was followed by overnight incubation in buffer with no zinc. This step was included to ensure that the evolving variants do not exhibit lower metal affinity.<sup>19</sup>

**Computationally Guided Library Design.** Although suitable for detection of detoxifying enzyme variants, the above assay is labor-intensive and amenable only to medium throughput ( $\sim 10^3$  variants). Thus, success was dependent on the design of small yet highly effective libraries. Given the wealth of previous engineering attempts of PTE, we commenced with a library based on mutations shown to improve PTE's activity with V-agents racemates and related surrogates.<sup>8,10,11,16–18,20–22</sup> However, combinations of known mutations yielded limited improvements for hydrolysis of the  $S_p$  isomers (see below). We therefore explored a combination of computational protein design with library selection: we used the Rosetta program to design libraries with sequence variation predicted to improve substrate interactions. We subsequently selected from these libraries the most active variants. In contrast with previous uses of Rosetta for the *de novo* design of enzymes,<sup>23,24</sup> the substrate binds to the starting scaffold, albeit weakly. Since this binding mode was not known, we iterated between computation and experiment: we started with an initial placement of transition state (TS) model based on structural and mechanistic knowledge of PTE, and after each round of selection refined this model using feedback from the experimental results; the refined model was then used in the next round of computational library design (supplementary Figure 1).

**Library Construction.** In constructing the libraries, we supplemented the Rosetta designed mutations with mutations known to modulate metal binding affinity and stability. The starting sequence was PTE-S5, a variant evolved for better expression than wild-type PTE in *E. coli*.<sup>25</sup> However, because PTE-S5 exhibits decreased metal affinity (Supplementary Figure 2; ref 25) our libraries included reversions of the three mutations in PTE-S5 relative to wild-type. Since function modifying mutations are destabilizing,<sup>26</sup> we included in all libraries six different mutations that were found to promote PTE's functional divergence with no effect on its enzymatic activities.<sup>19</sup> All of the above mutations reside far from the enzyme's active site.

Combinatorial libraries were generated by combining the stabilizing mutations with the designed active-site mutations using oligo spiking.<sup>27</sup> To maximize library efficiency,<sup>28</sup> the spiking level aimed at individual library variants carrying one or a maximum of two different active site mutations and  $\sim 3$  stabilizing mutations.

**First Round: G1.** We began with a library based on a combination of rationale and computational design (Table 1). Since our goal was to modify PTE's active site to accommodate both VX and RVX, we used a hybrid TS model with the bulkier *N,N*-diisopropyl head of the leaving group of VX (diethyl in RVX) and the bulkier alkoxy isobutyl group of RVX (*O*-ethyl in VX; Figure 1c). This hybrid TS was initially placed in the PTE active site in an orientation productive for hydrolysis by aligning the hydroxyl nucleophile of the TS with the hydroxyl ion bridging the metal atoms in PTE's crystal structure and enforcing an interaction between phosphoryl oxygen of the TS model and the  $\beta$ -metal ion (Supplementary Figure 3).

The active site sequence was then optimized for interactions with the bound TS model using RosettaDesign<sup>29</sup> with a bias for substitutions observed in related members of the amidohydrolase family (assuming that these exchanges would be better tolerated; for alignment see ref 30). The designed mutations

Table 2. Catalytic Rates of Nerve Agent Hydrolysis

variant	active site mutations	stabilizing mutations	$VX^b$ $S_p$	$VX^b$ $R_p$	$RVX^b$ $S_p$	$RVX^b$ $R_p$	$CVX^c$ $S_p$	amiton <sup>c</sup>	amiton- <i>N,N'</i> - $(iPr)_2$	Paraoxon <sup>d</sup>	$GA^e$ $S_p$	$GB^e$ $S_p$	$GD^e$ $S_p^f$	$GF^e$ $S_p$
PTE-SS (wild-type-like)			$0.94 \pm 0.07$ $0.98 \pm 0.27$	$0.68 \pm 0.02$	$0.06 \pm 0.01$ $0.07 \pm 0.13$	$2 \pm 0.13$	$0.14 \pm 0.01$ $0.23 \pm 0.02$	$0.56 \pm 0.02$	$1.36 \pm 0.21$	$232000 \pm 9000$	$69000 \pm 1400$	$823 \pm 68$	Fast $98 \pm 31$ Slow $11 \pm 2.8$	$4.8 \pm 0.8$
G1-C74	I106A, H254N	K77A, A80V, R185K, I274S, S319R	Fast <sup>g</sup> : $0.58 \pm 0.01$ slow <sup>g</sup> : $0.19 \pm 0.003$	Fast <sup>g</sup> : $0.01$ slow <sup>g</sup> : $0.01$	$1.9 \pm 0.01$ $3.3 \pm 0.7$	$0.67 \pm 0.002$	n.d.	$0.097 \pm 0.01$	$0.24 \pm 0.01$	n.d.	$2650 \pm 480$	$27 \pm 2$	$26 \pm 5$	$69 \pm 10$
G2-A137	I106A, F132E, H254G	K77A, A80V, A204G, G208D, I274S	$65 \pm 0.1$ $46 \pm 1.4$	$4.1 \pm 0.06$	$87 \pm 0.7$ $106 \pm 4$	$27 \pm 0.1$	n.d.	$2.52 \pm 0.11$	$2.98 \pm 0.07$	$19100 \pm 600$	n.d.	n.d.	n.d.	n.d.
G4-E36	I106V, F132E, H254G	K77A, A80V, G208D, I274N	$60 \pm 6.3$ $59.9 \pm 9$	$3.7 \pm 0.77$	$5.9 \pm 0.41$ $11.1 \pm 1$	$46 \pm 5.8$	n.d.	$5.11 \pm 0.89$	$8.85 \pm 0.35$	n.d.	n.d.	n.d.	n.d.	n.d.
G5-A53	I106A, F132E, T173Q, A203F, H254G	K77A, A80V, G208D, I274N	$175 \pm 0.8$ $300 \pm 45$	$20 \pm 1.4$	$347 \pm 7$ $343 \pm 54$	$68 \pm 7$	$132 \pm 40$ $265 \pm 58$	$9.5 \pm 0.42$	$23 \pm 1.6$	$22000 \pm 100$	$5380 \pm 190$	$3800 \pm 560$	$161 \pm 55$	$429 \pm 92$
G5-C23 <sup>h</sup>	F132E, T173N, H254G	K77A, A80V, G208D, I274N	$499 \pm 33$ $494 \pm 45$	$65 \pm 0.7$	$78 \pm 2.8$ $66 \pm 2$	$303 \pm 33$	$239 \pm 9$ $170 \pm 19$	$92 \pm 2$	$198 \pm 17$	$26900 \pm 1400$	$15800 \pm 1800$	$14800 \pm 2400$	$82.5 \pm 247$	$457 \pm 3$

<sup>a</sup>Underlined are the hydrolysis rates of the  $S_p$  isomers as determined by the AChE titration assay (detoxification rates). The hydrolysis rates of the  $R_p$  isomers were derived from the hydrolysis rates of the racemates (monitoring thiol release with DTNB) fitted to a biexponential model (resulting in a slow and fast rate constants). <sup>b</sup>The concentrations of VX, RVX, and CVX in the DTNB assay ranged from 18 to 25  $\mu$ M, and the variants were at 0.1–0.5  $\mu$ M (with the exception of PTE-SS and C74). C74 and the S5 were at 2–4.5  $\mu$ M. The concentrations of VX, RVX, and CVX in the detoxification assay ranged from 0.25 to 0.3  $\mu$ M, and the proteins were at 0.08–0.5  $\mu$ M. <sup>c</sup>The concentrations of amiton and amiton-*N,N'*-(*iPr*)<sub>2</sub> were 70 and 30  $\mu$ M, respectively. The proteins ranged from 1 to 4  $\mu$ M. <sup>d</sup>Paraoxon concentration was 10  $\mu$ M. PTE-SS protein concentration was 0.1–0.2 nM; variants A137, A53, and C23 concentrations ranged from 0.8 to 1.1 nM. <sup>e</sup>The concentrations of GA, GB, GD, and GF were 0.5, 0.3, 0.25, and 0.3  $\mu$ M, respectively. The variants A53 and C23 were at 0.001–0.03  $\mu$ M; C74 ranged from 0.02 to 1  $\mu$ M; PTE-SS ranged from 0.001 to 0.002  $\mu$ M when reacted with GA and biphasic behavior. <sup>f</sup>Only the DTNB assay was conducted, and thus the  $S_p$  and  $R_p$  hydrolysis rates could not be ascribed. <sup>g</sup>C23 variant also includes an unselected mutation P342S. It is located in a loop far from the active site and is thus unlikely to have a functional effect.

eliminated steric clashes and optimized packing with the TS model, particularly with the leaving group sulfur atom.

Approximately 1500 G1 library variants were screened for AChE protection against RVX (Supplementary Table 1). We chose RVX for the initial screen because a pocket accommodating RVX's alkoxy group would accept VX but not *vice versa*, and because we found that PTE detoxifies RVX 15-fold more slowly than VX (Table 2). Following the initial screen, the most active variants were assayed with both RVX and VX. Sequencing indicated the dominance of mutations of His254, mostly to Asn, alongside other mutations (Supplementary Table 2). The highest improvements were observed with VX with C74 being the only significantly improved variant for RVX detoxification. C74 carried a unique active site mutation I106A in concert with H254N (Table 2). The smaller Ala at 106 was suggested by the computational models to allow the accommodation of the larger isobutyl moiety of  $S_p$ -RVX (Supplementary Figure 4a). Hydrolysis rates measured with purified C74 indicated ~30-fold higher detoxification rates of RVX relative to wild-type and loss of the  $R_p$  preference (Table 2). Various stabilizing mutations were also readily adopted by all variants (Table 1).

**G2.** On the basis of the large RVX activity increase in the I106A mutant, we refined the modeled TS orientation keeping the alkoxy isobutyl group close to Ala106. The G2 computational library design focused on generating polar or charged interactions to the sulfur atom of the leaving group, which was presumed to be the main bottleneck of the reaction. The computation also explored potential interactions with the tertiary amine moiety of the leaving group (for a detailed explanation see Supporting Information). Mutations in positions proximal to the sulfur, *e.g.*, F306R, and to the *N*-dialkyl group, *e.g.*, F132D or E, were thus identified.

The library was supplemented with mutations at several additional positions. To test the modeled TS placement, we attempted to introduce the mutation M317W, which by the model resulted in a steric clash (Supplementary Figure 5). In addition, due to the dominance of mutations in 254 in G1, we mutated this position to all 20 amino acids. We also included mutations in His257 and Asp233, both of which are in proximity to 254 (second-shell optimization or 'neighbor joining'<sup>28</sup>).

To maintain broad-spectrum detoxification, we screened ~800 variants from G2 using an equimolar mixture of VX and RVX. All significantly improved variants included substitutions of Phe132 to either Asp or Glu (Supplementary Table 2). The AChE protection conferred by these variants appeared to be higher against all three V-agents. Variant H81 (active site mutations H254N, I106A, F132E), for example, had a clear preference of the toxic  $S_p$  isomers (*ca.* 8-fold faster rates than with  $R_p$ ) and  $k_{cat}/K_M$  values of 0.5 and  $2.3 \times 10^5 \text{ M}^{-1} \text{ min}^{-1}$  for VX and RVX, respectively (Supplementary Table 3).

As described above, the F132D/E substitutions were computationally designed to interact with the V-agents choline-like *N*-dialkyl group. Phe132 lies within a hydrophobic patch of PTE's active-site wall, and the Asp/Glu carboxylates were predicted to interact electrostatically with the *N*-dialkyl group, thus better aligning the  $S_p$  isomers within the active-site (Figure 3). In agreement with this model, the F132D/E mutations increased the rate for the  $S_p$  isomers of both VX and RVX by  $\geq 10$ -fold but had little effect on the rate of hydrolysis of  $R_p$  VX/RVX (Supplementary Table 3) and on a VX analogue with a phenyl leaving group (specified below). The modeled TS

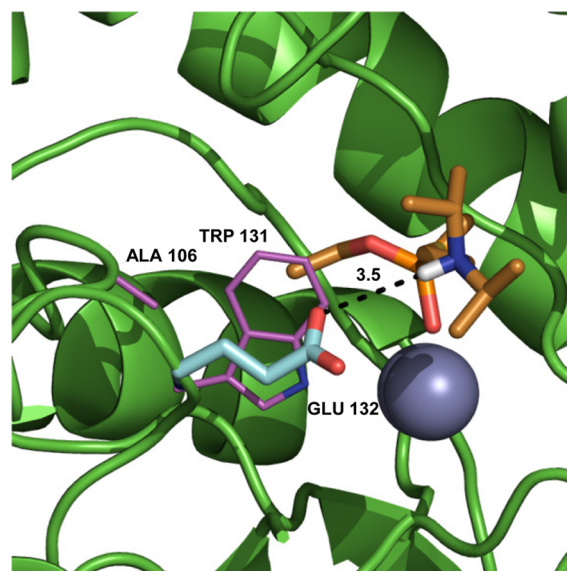


**Figure 3.** Predicted interaction between the designed Glu132 and the choline-like group of VX. Glu132 (cyan) forms a charge–charge interaction with the tertiary amine of the *N,N*-diisopropyl group. Trp131 (magenta) resides underneath Glu132. Also shown is the side chain of residue Ala106 (magenta) that accommodates the *O*-alkyl group.

orientation was further supported by the absence of the M317W and M317A substitutions in all improved variants.

The other highly improved G2 variant, A137, was identical to H81 except that His254 was mutated to Gly instead of Asn. Its detoxification rates were ~5-fold faster than those of H81, and its  $k_{cat}/K_M$  for  $S_p$ -VX approached  $10^6 \text{ M}^{-1} \text{ min}^{-1}$  (Table 2, Figure 4). The  $R_p$  isomers of both VX and RVX were hydrolyzed 10-fold faster (Table 2). The design model suggests that replacement of the bulky His by Gly enables better accommodation of V-agents, but Gly254 may also affect the conformational ensemble and dynamics of loop 7 (residues 250–295), thereby modulating substrate binding.<sup>30</sup> G2 variants also contained stabilizing mutations including the S5 reversion mutation G208D. Accordingly, despite carrying three active-site mutations, the levels of soluble expression of the evolved variants were similar. The metal complex stability was also improved by  $>10^3$ -fold relative to PTE-S5 (Supplementary Figure 2).

**G3.** The G2 results showed that stabilizing mutations were accommodated alongside the active site substitutions. We thus sought to include in the G3 library additional stabilizing mutations (Table 1). However, besides I274N,<sup>31</sup> we had exhausted the repertoire of known stabilizing mutations. Hence we used Rosetta to identify potential stabilizing substitutions, primarily by improving local packing. At the active site, in the G3 library we explored position 131, which neighbors the key G2 mutation F132E, and also attempted to replace acidic Glu132 with the hydrophobic Ile that had been reported to be advantageous.<sup>7</sup> Screening of ~250 variants (with an equimolar mixture of VX and RVX; Table 1) yielded no further improvements exceeding those of the best G2 variants. Sequencing revealed that Trp131 was irreplaceable, and Glu132 remained the best option, thus supporting the computational model. Among the computationally guided stabilizing mutations, T147Y occurred in many active variants (Supplementary Table 2). This mutation is predicted to increase the local packing against Leu151 (Supplementary Figure 6).

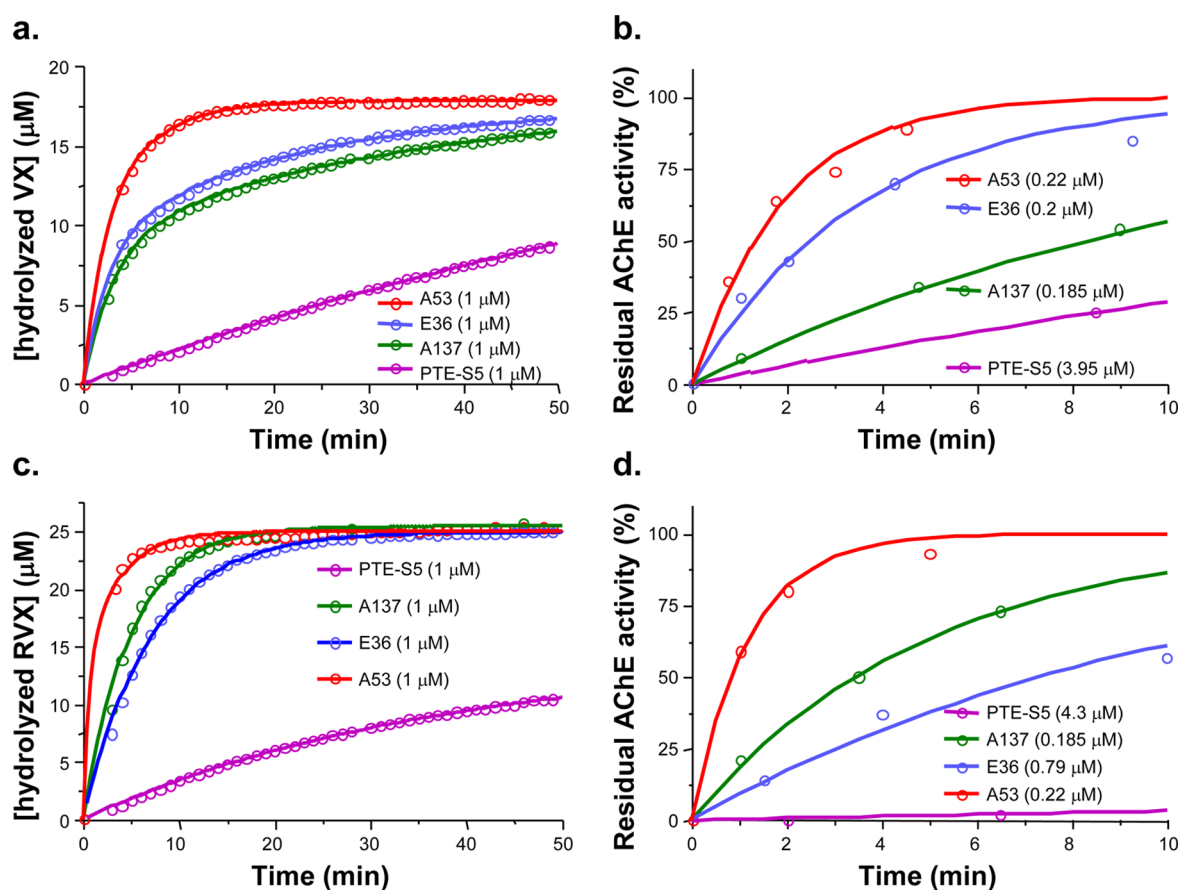


**Figure 4.** Hydrolysis of VX by PTE variants. Hydrolysis of racemic VX (a) or RVX (c) by wild-type (PTE-S5) and variants A137, E36, A53. The release of the thiol leaving group was monitored with Ellman's reagent. The rates of detoxification were determined by measuring residual AChE activity following incubation of PTE variants with racemic VX (b) or RVX (d) for different time periods. Data were fitted to a first-order rate equation to derive the apparent rate constant for hydrolysis of the  $S_p$  isomer. A time period of 10 min is shown for all variants, but the rates for PTE-S5 and A137 were derived from multiple time points over 90 and 20 min, respectively.

**G4.** The G4 library was based on a refined model of TS binding. In particular, based on the increased activity of F132E and the I106A mutants, the TS model was placed such that the leaving group's *N*-dialkylamine moiety interacts with Glu132, and with the isobutyl moiety of  $S_p$ -RVX close to Ala106. Rosetta was then used to search for mutations predicted to interact with the bound V-agents in the refined model. Mutations in positions neighboring the interacting residues, and in positions that could affect the configuration of the active-site loops, were also included (Table 1).

Given the relatively high detoxification rates of the starting point (G3 variants), we screened separately with VX and RVX, such that specialist variants would not be overlooked. A total of ~700 variants were screened. A number of highly active variants were identified (Supplementary Table 2), with the best two variants, E36 and I19, showing only small improvements relative to A137 (Supplementary Table 3). Variant E36 became specialized in  $S_p$ -VX ( $k_{cat}/K_M = 6 \times 10^5 \text{ M}^{-1} \text{ min}^{-1}$ ) as its rate with  $S_p$ -RVX was 10-fold slower (Table 2 and Figure 4). This effect was produced by the I106V mutation (instead of I106A in A137 and generalist variants). Indeed, the model indicated that Val106 provides improved packing of  $S_p$ -VX's *O*-ethyl group but clashes with the larger isobutyl group of  $S_p$ -RVX (Supplementary Figure 4b). Conversely, variant I19, carrying I106A as well as D233M, showed 40-fold higher detoxification

rates for RVX over VX ( $k_{cat}/K_M$  of  $3.6 \times 10^5$  and  $0.8 \times 10^4 \text{ M}^{-1} \text{ min}^{-1}$ , respectively; Supplementary Table 3).

**G5.** For G5, the computational models were further refined on the basis of the four preceding rounds as well as the kinetic data with the different stereoisomers. The refined model suggested that mutations at two new positions, Thr173 and Ala203, could improve binding of the choline-like moiety of V-agents and reinforce the effect of Glu132. Furthermore, since PTE's recent divergence from a lactonase involved a point mutation in 254 that enabled a 9-residue insertion within loop7 (residues Asn263 to Gly273),<sup>30</sup> we explored single amino acid deletions within this segment in parallel with further diversification at 254 (the previously selected Gly and Asn, and other polar amino acids, Ser, Thr).

Screening of ~400 variants resulted in the isolation of several highly active clones (Supplementary Table 3). These carried a range of new mutations including T173N/Q/W, A203F/L, H254S, and a deletion of A266 (Supplementary Table 2). Among the most active ones, A53 variant maintained a generalist character, detoxifying VX, RVX and CVX with similar rates (Table 2 and Figure 4). This variant carried the same active site mutations of A137 (I106A, F132E and H254G) and two new mutations, T173Q and A203F. The latter were designed to promote interactions with the choline-like moiety (Figure 5). In contrast, variant C23 exhibited the fastest rate for VX detoxification ( $\sim 5 \times 10^6 \text{ M}^{-1} \text{ min}^{-1}$ ) but a lower rate with  $S_p$ -CVX

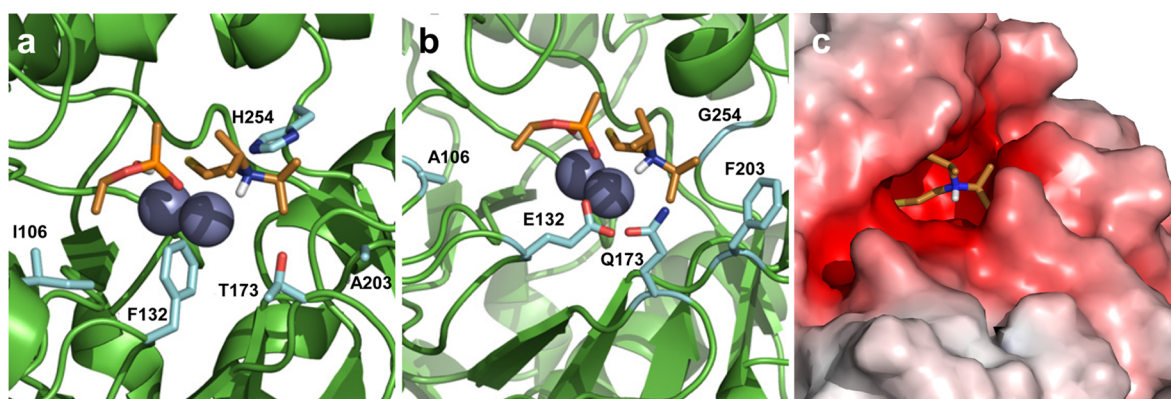


**Figure 5.** Computational models of wild-type PTE (a) and the 5th generation variant A53 (b) with the bound substrate model (the  $S_P$  isomer of a VX-RVX hybrid; Figure 1c). (c) The designed pocket of the A53 variant is complementary to VX's leaving group, including charge complementarity to the choline-like moiety.

**Table 3. Catalytic Rates of V-Agent Analogue Hydrolysis<sup>a</sup>**

variant	$K_{cat}/K_M$ ( $M^{-1} \text{ min}^{-1} \pm \text{SD}$ )				O/S rates ratio <sup>b</sup>	
	$\text{CH}_3(\text{EtO})\text{P}(=\text{O})\text{-O-coumarin}$		$\text{CH}_3(\text{EtO})\text{P}(=\text{O})\text{-S-phenyl}$		fast	slow
	fast	slow	fast	slow		
PTE-S5	$81.5 \pm 4.0 \times 10^7$		$36 \pm 5 \times 10^4$		2263	
G5-B60	$101.5 \pm 26 \times 10^7$	$40.5 \pm 13.4 \times 10^7$	$33 \pm 3.8 \times 10^4$	$11 \pm 1.7 \times 10^4$	3075	3681
G5-A57	$17.5 \pm 0.9 \times 10^7$		$16 \pm 1 \times 10^4$		1069	
G5-B84	$28.8 \pm 7.3 \times 10^7$	$13.5 \pm 0.42 \times 10^7$	$13 \pm 1.4 \times 10^4$	$3.6 \pm 0.1 \times 10^4$	2215	3750
G5-G23	$10.4 \pm 1.56 \times 10^7$	$8.05 \pm 1.8 \times 10^7$	$4.8 \pm 1.3 \times 10^4$		2166	1677
G5-A53	$8.1 \pm 1.4 \times 10^7$	$6.25 \pm 1.2 \times 10^7$	$3.8 \pm 0.5 \times 10^4$	$3.1 \pm 0.5 \times 10^4$	2130	1644
G5-C23	$56.1 \pm 4.1 \times 10^7$	$24.6 \pm 8.2 \times 10^7$	$21 \pm 3.2 \times 10^4$	$10 \pm 0.7 \times 10^4$	2671	2460

<sup>a</sup>These surrogates contain the *O*-ethyl methylphosphonyl group of VX ( $\text{CH}_3(\text{EtO})\text{P}(=\text{O})\text{-}$ ) with two different leaving groups replacing the  $\text{-S-CH}_2\text{-CH}_2\text{-N}(\text{iPr})_2$  leaving group of VX: an oxo leaving group ( $\text{-O-coumarin}$ ) and a thio one ( $\text{-S-phenyl}$ ), both having the same  $\text{p}K_a$ . <sup>b</sup>The ratio between the oxo-ester and thio-ester hydrolysis rates.

( $\sim 2 \times 10^6 \text{ M}^{-1} \text{ min}^{-1}$ ) and  $S_P$ -RVX ( $0.7 \times 10^6 \text{ M}^{-1} \text{ min}^{-1}$ ). Further, C23 was singular in hydrolyzing the  $R_P$  isomer of RVX with >4-fold faster rates than  $S_P$  isomer. The specialization toward VX appears to be explained by having Ile rather than Ala at position 106. In the case of CVX, the  $S_P$  preference is maintained owing to the less bulky *O*-*n*-butyl moiety. Overall, G5 variants represent a >5,000 fold increase in the rates of PTE's detoxification of RVX, >1,000-fold improvement in CVX and >500-fold increase for VX.

**Surrogates and Origins of Optimization.** We tested a series of analogues of V-agents, including analogues that are amenable to high-throughput screens. We varied either the phosphonate or leaving group moieties (Supplementary Figure 7; Table 3). This analysis made it clear that the optimization toward V-agent detoxification does not consistently correlate with higher rates of hydrolysis with any of the tested analogues. For example, the rates of hydrolysis of a fluorogenic oxo-ester with an *O*-ethyl-methylphosphonate group identical to VX ( $\text{CH}_3(\text{EtO})\text{P}(=\text{O})\text{-O-Coumarin}$ ) decreased in the evolved variants. The rates with the respective thiophenyl ester ( $\text{CH}_3(\text{EtO})\text{P}(=\text{O})\text{-S-phenyl}$ ) were also reduced. Consequently, the thio-effect remained as high as in wild-type PTE (Table 3).

The analysis of analogues also indicated that the catalytic chemistry and the recognition of the phosphonate moiety were not significantly altered. Rather, the computationally designed pocket seems to recognize the tertiary-ammonium moieties of V-agents (Figure 5), a feature that is completely absent in wild-type PTE. Specifically, the hydrolysis rates with various

combinations of *O*-alkyl phosphonate ( $\text{CH}_3(\text{RO})\text{P}(=\text{O})\text{-}$ ) and different *N*-alkyl choline-like leaving groups ( $\text{-SCH}_2\text{CH}_2\text{NR}'_2$ ; Figure 1; Table 3) indicate that the designed F132E mutation, and the designed changes at 173 and 203 that followed appear to be crucial for recognition of the choline-like leaving group. The interactions with the choline-like moiety increase the rates of hydrolysis and also dictate the  $S_P$  stereospecificity. This is manifested in G5 variants showing up to  $\sim 150$ -fold higher rates relative to wild-type with amiton and amiton-*N,N*-diisopropyl analogue - diethylphosphoro esters with the same leaving group as VX and RVX, respectively (Figure 1; Table 2). Taken together with a concomitant  $\sim 10$ -fold decrease in rates with paraoxon (diethylphosphoro ester with *p*-nitrophenyl leaving group), it is evident that the active site of the G5 variants was reshaped to accommodate the choline-like leaving group, particularly in the  $S_P$  configuration (Figure 5). Further, minor improvements in amiton rates were observed in G1–G4 variants, suggesting a key role for the mutations at 173 and 203 in shaping the complex with the  $S_P$  substrate configuration.

**G-Agent Detoxification.** Having obtained broad-spectrum V-agents hydrolases, we also evaluated the detoxification rates of G-agents (Figure 1; Table 2). G-agents with bulky *O*-alkyl groups, GD or GF, are not effectively detoxified by wild-type PTE. However, G5 variants exhibited up to 100-fold rate improvements for their  $S_P$  isomers, thus approaching  $k_{cat}/K_M$  values of  $8 \times 10^6 \text{ M}^{-1} \text{ min}^{-1}$ . Rates of detoxification of the less bulky agents, GA and GB, were reduced relative to wild-type, but G5 variants are sufficiently active for effective *in vivo*

detoxification ( $k_{\text{cat}}/K_{\text{M}} > 10^8 \text{ M}^{-1} \text{ min}^{-1}$ ). The improved detoxification rates with G-agents is likely due to changes at positions 254 and 106, which are present in PTE variants that exhibit improved rates with G-agents including GF.<sup>7,11</sup>

**Implications for Broad-Spectrum Detoxification.** We report the generation of PTE variants capable of hydrolyzing the toxic isomer of all known V-type as well as G-type nerve agents with  $k_{\text{cat}}/K_{\text{M}}$  values  $\geq 2.5 \times 10^6 \text{ M}^{-1} \text{ min}^{-1}$  (Table 2 and Supplementary Table 3). While protection at low enzyme doses ( $\leq 1 \text{ mg kg}^{-1} \text{ body}$ ) demands further rate improvements ( $k_{\text{cat}}/K_{\text{M}} > 10^7 \text{ M}^{-1} \text{ min}^{-1}$ ), having one variant, or two closely related PTE variants, that detoxify the entire range of agents, seems within reach. Broad spectrum is crucial as the threat's identity is rarely known in advance (for prophylaxis) or even after exposure (for post-treatment, e.g., following skin exposure to V-agents). Mixtures of agents were also used in the past.

**Concluding Remarks.** Our integrated computational and experimental approach was quite effective. While protein design capabilities are improving, predicting a single sequence that confers high catalytic efficiency is still out of reach. The design tools are, however, sufficiently advanced to focus the search. Thus, highly efficient catalysts could be identified and subsequently refined by screening several hundreds of variants per round. A focused search has proven essential for the task in hand. Nontoxic surrogates, with a chromogenic leaving group as well as  $S_{\text{P}}$  stereochemistry, that enable high-throughput screening failed to consistently report activity with the  $S_{\text{P}}$  isomers of the actual agents (Tables 2 and 3). Given the minimal screening capacity, the Rosetta-based models comprised a useful guiding tool. The modeling enabled us to have a reasonable structural model and, specifically, to model the binding mode of V-agents within PTE's active site, as well as to identify mutations that reinforce this mode.

We note, however, that our interpretations are based on the computational models. These ultimately must be validated by crystal structures of the evolved variants with suitable V-agent analogues. Nonetheless, comparison of the rates with different surrogates and V-agents and with their  $R_{\text{P}}$  and  $S_{\text{P}}$  isomers suggests that our primary aim of designing an 'anionic pocket' for the V-agents' choline-like moiety may have been achieved (Figure 5). Interestingly, a carboxylate-based electrostatic interaction was originally predicted for AChE and the acetylcholine receptor, hence the term 'anionic pocket'. The structures, however, revealed that recognition is based on pi-cation interactions mediated by an 'aromatic box'.<sup>32</sup> Recognition of the choline-like moiety in the designed PTE variants was based on both elements (Figure 5), since both Glu132 and Trp131 were proven essential. Indeed, the F132E has not been identified in a parallel study aimed at engineering PTE for high VX hydrolysis rates.<sup>12</sup> In summary, we expect that this work (as well as subsequent attempts to optimize the detoxification rate of PTE), along with current and future computational redesign studies<sup>33,34</sup>—will allow the establishment of a robust protocol for computationally aided enzyme optimization. Overall, the design of 'small and smart' libraries is becoming increasingly crucial as the field of enzyme engineering begins to tackle increasingly challenging tasks.

## METHODS

**Library Construction.** Libraries derived from PTE-SS, within the pMAL-c2x vector, were constructed as described.<sup>30</sup> Also see Supporting Information for more details.

**Screening.** Randomly picked colonies from fresh transformation were individually grown in 96-well plates, at 30 °C with shaking, using 0.5 mL of LB medium with 100  $\mu\text{g}/\text{mL}$  ampicillin. Overnight cultures were used to inoculate (1:100 dilution) 0.5 mL of LB medium with 100  $\mu\text{g}/\text{mL}$  ampicillin and 0.1 mM  $\text{ZnCl}_2$ . Following growth to  $\text{OD}_{600 \text{ nm}} \approx 0.8$ , expression was induced with 0.4 mM IPTG, and growth at 30 °C was continued for another 16 h. Cells were centrifuged and lysed by shaking in 0.1 M Tris pH 8.0, 0.1 M NaCl, 0.1% v/v Triton X100 and 0.2 mg  $\text{mL}^{-1}$  lysozyme. Lysates were centrifuged and kept at 4 °C for 1–3 overnights before screening. To screen for hydrolysis of the  $S_{\text{P}}$  isomer, the reaction mixture included 50  $\mu\text{L}$  of lysate, 10  $\mu\text{L}$  of *in situ* generated V-agents and 40  $\mu\text{L}$  of AChE (final concentrations are given in Supplementary Table 1). In G1 and G2, AChE was added after 30 min incubation of the lysate plus NA, whereas in G3–G5, the NA was added to the lysate plus AChE. In all cases, the final reaction mixtures were incubated for 60 min before determination of residual AChE activity. For the latter, 20  $\mu\text{L}$  was added to 180  $\mu\text{L}$  of PBS containing 0.85 mM dithionitrobenzoic acid (DTNB) and 0.55 mM acetylthiocholine.

**Expression and Purification.** LB medium including ampicillin was inoculated with a single colony of freshly transformed *E. coli* BL21 and grown overnight at 30 °C. Inoculates were added (1:100 dilution) to 100 mL of LB with ampicillin and 0.2 mM  $\text{ZnCl}_2$  and grown at 37 °C to  $\text{OD}_{600 \text{ nm}} \approx 0.8$ . IPTG was added (0.4 mM), and cultures were grown overnight at 20 °C. Cells were harvested by centrifugation and resuspended with 10 mL of buffer A (100 mM Tris pH 8.0, 0.1 M NaCl, 10 mM  $\text{NaHCO}_3$ , 1:500 diluted protease inhibitor cocktail (Sigma), 50 units of Benzonase, 0.1 mM  $\text{ZnCl}_2$ ). Cells were lysed using sonication, clarified by centrifugation, and passed through an amylose column (NEB) pre-equilibrated with buffer A. Following extensive wash with buffer A, the MBP–PTE fusion protein was eluted with buffer A plus 10 mM maltose and 0.1 mM  $\text{ZnCl}_2$ . Enzyme containing fractions were combined and stored at 4 °C. Purity and protein concentrations were determined by SDS–PAGE and absorbance at 280 nm (extinction coefficient 95925  $\text{M}^{-1}\text{cm}^{-1}$ ). Then, zinc was removed by buffer exchange, and samples were stored at 4 °C until analysis. Enzyme activity was stable for months.

**Metal Stability Assay.** The assay was performed essentially as described,<sup>25</sup> using 50 mM Tris pH 8.0, 50 mM NaCl buffer. See Supporting Information for specific details.

**Enzyme Kinetics.** Hydrolysis rates ( $k_{\text{cat}}/K_{\text{M}}$ ) of V-agent racemates and analogues thereof were monitored by following the release of the thio leaving group using the Ellman's reagent (DTNB assay) (Figure 1c) as described.<sup>6,35</sup> The kinetic parameters of individual variants were determined by fitting the kinetic data directly to a two-phase decay equation<sup>36</sup> using GraphPad Prism version 5.00 Software.<sup>37</sup> See Supporting Information for details and equations used for data analysis. The hydrolysis rates ( $k_{\text{cat}}/K_{\text{M}}$ ) of the  $S_{\text{P}}$  isomers were determined using the AChE assay, essentially as described.<sup>6</sup> Accordingly, the individual variants were incubated with the target OP, and samples were taken at various time points to determine the residual OP concentration. This was achieved by reacting the samples with AChE and measuring the residual AChE activity (i.e., measuring the decrease in AChE inhibition level). The % activity values were plotted on an exponential scale to derive the  $k_{\text{cat}}/K_{\text{M}}$  from the slope of the single exponential curves<sup>36</sup> using GraphPad Prism Software.<sup>37</sup> See 'enzyme kinetics' in Supporting Information for specific details and equation used.

**Computational Design.** We assumed that OP hydrolysis proceeds through an inline nucleophilic attack by hydroxide on the phosphorus atom, with a trigonal bipyramidal transition state geometry.<sup>38</sup> Structures of VX, RVX, and CVX were generated as  $S_{\text{P}}$  stereoisomers and used to generate the TS models.<sup>39</sup> These were constructed by keeping the trigonal bipyramidal geometry of the phosphorus while varying the lengths of the bonds being formed (HO–P) and broken (P–S; Supplementary Figure 8). In the initial rounds of design, TS models were superimposed onto PTE's binuclear metal site from crystal structures (for G1, PDB accession codes: 2R1K, 1EZ2; for G2: 1DPM, 1HZY) using nonprotein residues – water molecules and ligands coordinating the metal site. In the later rounds of designs, G4 and G5, the TS models of the substrate were varied

around the zinc site (see Supporting Information). The coordination geometry of the metal site was preserved by imposing restraints on the metal ions and its coordinating amino acid side chains (including the crystallographic rotameric states). Rotamer ensembles of the TS models were generated using OpenEye's Omega software<sup>40</sup> preserving the geometry around the phosphorus atom to enhance sampling. We searched for specific interactions to the developing negative charge of the leaving group's sulfur atom using the RosettaMatch algorithm.<sup>41</sup> Acidic and pi interactions to the N-alkyl moiety were similarly explored. TS models and protein interactions were optimized using RosettaDesign,<sup>29</sup> by exploring new sequences that better accommodate the TS model and the newly introduced TS-specific interactions. This process was iterative, and the models were updated from one round to another on the basis of the experimental results (Supplementary Figure 1). Stabilizing mutations were computed on the basis of PDB accession code 1DPM into which known stabilizing mutations (Table 1) were modeled. The model was minimized with restraints on the rotameric configuration of side chains 55, 57, 210, 211, 213, 214, 215, 217, 218, 219, 220, 221, 222, 223, 224, 225, 230, and 301 and of the interactions between the metals and their coordinating residues. Energy minimization was done in the absence of ligand but with the two zinc atoms and the bridging hydroxide present. Next, all residues were singly substituted to all 20 amino acids. Each substitution was followed by gradient-based steepest descent minimization and calculation of the change in total energy. Potentially stabilizing substitutions were recomputed, and the five lowest energy substitutions were included in the libraries.

## ■ ASSOCIATED CONTENT

### ● Supporting Information

Experimental procedures and supplementary figures and tables. This material is available free of charge via the Internet at <http://pubs.acs.org>.

### Accession Codes

PDB: 2R1K, 1E2Z, 1DPM, 1HZY.

## ■ AUTHOR INFORMATION

### Corresponding Authors

\*E-mail: [dabaker@u.washington.edu](mailto:dabaker@u.washington.edu).

\*E-mail: [dan.tawfik@weizmann.ac.il](mailto:dan.tawfik@weizmann.ac.il).

### Author Contributions

§These authors contributed equally to this work.

### Notes

The authors declare no competing financial interest.

## ■ ACKNOWLEDGMENTS

Financial support by DTRA (HDTRA1-11-C-0026) is gratefully acknowledged. D.S.T. is the Nella and Leon Benozio Professor of Biochemistry. P.J.G. was supported by Carlsberg-fondet and EMBO Long-term postdoctoral fellowship.

## ■ REFERENCES

- (1) Bajgar, J. (2005) Complex view on poisoning with nerve agents and organophosphates. *Acta Med. (Hradec Kralove, Czech Repub.)* 48, 3–21.
- (2) Ashani, Y., and Pistinner, S. (2004) Estimation of the upper limit of human butyrylcholinesterase dose required for protection against organophosphates toxicity: a mathematically based toxicokinetic model. *Toxicol. Sci.* 77, 358–367.
- (3) Lenz, D. E., Yeung, D., Smith, J. R., Sweeney, R. E., Lumley, L. A., and Cerasoli, D. M. (2007) Stoichiometric and catalytic scavengers as protection against nerve agent toxicity: a mini review. *Toxicology* 233, 31–39.
- (4) Ashani, Y., Goldsmith, M., Leader, H., Silman, I., Sussman, J. L., and Tawfik, D. S. (2011) In vitro detoxification of cyclosarin in human

blood pre-incubated ex vivo with recombinant serum paraoxonases. *Toxicol. Lett.* 206, 24–28.

(5) Serdar, C. M., Gibson, D. T., Munnecke, D. M., and Lancaster, J. H. (1982) Plasmid Involvement in Parathion Hydrolysis by *Pseudomonas diminuta*. *Appl. Environ. Microbiol.* 44, 246–249.

(6) Goldsmith, M., Ashani, Y., Simo, Y., Ben-David, M., Leader, H., Silman, I., Sussman, J. L., and Tawfik, D. S. (2012) Evolved stereoselective hydrolases for broad-spectrum G-type nerve agent detoxification. *Chem. Biol.* 19, 456–466.

(7) Tsai, P. C., Fox, N., Bigley, A. N., Harvey, S. P., Barondeau, D. P., and Raushel, F. M. (2012) Enzymes for the homeland defense: optimizing phosphotriesterase for the hydrolysis of organophosphate nerve agents. *Biochemistry* 51, 6463–6475.

(8) Reeves, T. E., Wales, M. E., Grimsley, J. K., Li, P., Cerasoli, D. M., and Wild, J. R. (2008) Balancing the stability and the catalytic specificities of OP hydrolases with enhanced V-agent activities. *Protein Eng., Des. Sel.* 21, 405–412.

(9) Rastogi, V. K., DeFrank, J. J., Cheng, T. C., and Wild, J. R. (1997) Enzymatic hydrolysis of Russian-VX by organophosphorus hydrolase. *Biochem. Biophys. Res. Commun.* 241, 294–296.

(10) Briseno-Roa, L., Timperley, C. M., Griffiths, A. D., and Fersht, A. R. (2011) Phosphotriesterase variants with high methylphosphonate activity and strong negative trade-off against phosphotriesters. *Protein Eng., Des. Sel.* 24, 151–159.

(11) Tsai, P. C., Bigley, A., Li, Y., Ghanem, E., Cadieux, C. L., Kasten, S. A., Reeves, T. E., Cerasoli, D. M., and Raushel, F. M. (2010) Stereoselective hydrolysis of organophosphate nerve agents by the bacterial phosphotriesterase. *Biochemistry* 49, 7978–7987.

(12) Bigley, A. N., Xu, C., Henderson, T. J., Harvey, S. P., and Raushel, F. M. (2013) Enzymatic neutralization of the chemical warfare agent VX: Evolution of phosphotriesterase for phosphorothiolate hydrolysis. *J. Am. Chem. Soc.* 135, 10426–10432.

(13) Schofield, D. A., and Dinovo, A. A. (2010) Generation of a mutagenized organophosphorus hydrolase for the biodegradation of the organophosphate pesticides malathion and demeton-S. *J. Appl. Microbiol.* 109, 548–557.

(14) Jeong, Y. S., Choi, S. L., Kyeong, H. H., Kim, J. H., Kim, E. J., Pan, J. G., Rha, E., Song, J. J., Lee, S. G., and Kim, H. S. (2012) High-throughput screening system based on phenolics-responsive transcription activator for directed evolution of organophosphate-degrading enzymes. *Protein Eng., Des. Sel.* 25, 725–731.

(15) Omburo, G. A., Kuo, J. M., Mullins, L. S., and Raushel, F. M. (1992) Characterization of the zinc binding site of bacterial phosphotriesterase. *J. Biol. Chem.* 267, 13278–13283.

(16) Chen-Goodspeed, M., Sogorb, M. A., Wu, F., Hong, S. B., and Raushel, F. M. (2001) Structural determinants of the substrate and stereochemical specificity of phosphotriesterase. *Biochemistry* 40, 1325–1331.

(17) Briseno-Roa, L., Olynyk, Z., Timperley, C. M., Griffiths, A. D., and Fersht, A. R. (2011) Highest paraoxonase turnover rate found in a bacterial phosphotriesterase variant. *Protein Eng., Des. Sel.* 24, 209–211.

(18) Kuo, J. M., Chae, M. Y., and Raushel, F. M. (1997) Perturbations to the active site of phosphotriesterase. *Biochemistry* 36, 1982–1988.

(19) Tokuriki, N., Jackson, C. J., Afriat-Jurnou, L., Wyganowski, K. T., Tang, R., and Tawfik, D. S. (2012) Diminishing returns and tradeoffs constrain the laboratory optimization of an enzyme. *Nat. Commun.* 3, 1257.

(20) Watkins, L. M., Mahoney, H. J., McCulloch, J. K., and Raushel, F. M. (1997) Augmented hydrolysis of diisopropyl fluorophosphate in engineered mutants of phosphotriesterase. *J. Biol. Chem.* 272, 25596–25601.

(21) Hill, C. M., Li, W. S., Thoden, J. B., Holden, H. M., and Raushel, F. M. (2003) Enhanced degradation of chemical warfare agents through molecular engineering of the phosphotriesterase active site. *J. Am. Chem. Soc.* 125, 8990–8991.

(22) Hoskin, F. C., Walker, J. E., Dettbarn, W. D., and Wild, J. R. (1995) Hydrolysis of tetriso by an enzyme derived from *Pseudomonas*

diminuta as a model for the detoxication of O-ethyl S-(2-diisopropylaminoethyl) methylphosphonothiolate (VX). *Biochem. Pharmacol.* 49, 711–715.

(23) Khare, S. D., Kipnis, Y., Greisen, P., Jr., Takeuchi, R., Ashani, Y., Goldsmith, M., Song, Y., Gallaher, J. L., Silman, I., Leader, H., Sussman, J. L., Stoddard, B. L., Tawfik, D. S., and Baker, D. (2012) Computational redesign of a mononuclear zinc metalloenzyme for organophosphate hydrolysis. *Nat. Chem. Biol.* 8, 294–300.

(24) Richter, F., Leaver-Fay, A., Khare, S. D., Bjelic, S., and Baker, D. (2011) De novo enzyme design using Rosetta3. *PLoS One* 6, e19230.

(25) Roodveldt, C., and Tawfik, D. S. (2005) Directed evolution of phosphotriesterase from *Pseudomonas diminuta* for heterologous expression in *Escherichia coli* results in stabilization of the metal-free state. *Protein Eng., Des. Sel.* 18, 51–58.

(26) Tokuriki, N., and Tawfik, D. S. (2009) Stability effects of mutations and protein evolvability. *Curr. Opin. Struct. Biol.* 19, 596–604.

(27) Herman, A., and Tawfik, D. S. (2007) Incorporating synthetic oligonucleotides via gene reassembly (ISOR): a versatile tool for generating targeted libraries. *Protein Eng., Des. Sel.* 20, 219–226.

(28) Goldsmith, M., and Tawfik, D. S. (2013) Enzyme engineering by targeted libraries. *Methods Enzymol.* 523, 257–283.

(29) Kuhlman, B., and Baker, D. (2000) Native protein sequences are close to optimal for their structures. *Proc. Natl. Acad. Sci. U.S.A.* 97, 10383–10388.

(30) Afriat-Jurnou, L., Jackson, C. J., and Tawfik, D. S. (2012) Reconstructing a missing link in the evolution of a recently diverged phosphotriesterase by active-site loop remodeling. *Biochemistry* 51, 6047–6055.

(31) Mee-Hie Cho, C., Mulchandani, A., and Chen, W. (2006) Functional analysis of organophosphorus hydrolase variants with high degradation activity towards organophosphate pesticides. *Protein Eng., Des. Sel.* 19, 99–105.

(32) Dougherty, D. A. (2013) The cation-pi interaction. *Acc. Chem. Res.* 46, 885–893.

(33) Voigt, C. A., Mayo, S. L., Arnold, F. H., and Wang, Z. G. (2001) Computational method to reduce the search space for directed protein evolution. *Proc. Natl. Acad. Sci. U.S.A.* 98, 3778–3783.

(34) Privett, H. K., Kiss, G., Lee, T. M., Blomberg, R., Chica, R. A., Thomas, L. M., Hilvert, D., Houk, K. N., and Mayo, S. L. (2012) Iterative approach to computational enzyme design. *Proc. Natl. Acad. Sci. U.S.A.* 109, 3790–3795.

(35) Gupta, R. D., Goldsmith, M., Ashani, Y., Simo, Y., Mullochandov, G., Bar, H., Ben-David, M., Leader, H., Margalit, R., Silman, I., Sussman, J. L., and Tawfik, D. S. (2011) Directed evolution of hydrolases for prevention of G-type nerve agent intoxication. *Nat. Chem. Biol.* 7, 120–125.

(36) Laidler, K. J. (1965) *Chemical Kinetics*, McGraw-Hill, Inc, New York.

(37) *GraphPad Prism version 5.00 for Windows*, GraphPad Software, San Diego, CA; [www.graphpad.com](http://www.graphpad.com).

(38) Aubert, S. D., Li, Y., and Raushel, F. M. (2004) Mechanism for the hydrolysis of organophosphates by the bacterial phosphotriesterase. *Biochemistry* 43, 5707–5715.

(39) Peterson, M. W., Fairchild, S. Z., Otto, T. C., Mohtashemi, M., Cerasoli, D. M., and Chang, W. E. (2011) VX hydrolysis by human serum paraoxonase 1: a comparison of experimental and computational results. *PLoS One* 6, e20335.

(40) Bostrom, J., Greenwood, J. R., and Gottfries, J. (2003) Assessing the performance of OMEGA with respect to retrieving bioactive conformations. *J. Mol. Graphics Modell.* 21, 449–462.

(41) Zanghellini, A., Jiang, L., Wollacott, A. M., Cheng, G., Meiler, J., Althoff, E. A., Rothlisberger, D., and Baker, D. (2006) New algorithms and an in silico benchmark for computational enzyme design. *Protein Sci.* 15, 2785–2794.